

1994019692

329

N94-241765

Effects of shock strength on shock turbulence interaction

By Sangsan Lee

Direct numerical simulation (DNS) and linear analysis (LIA) of isotropic turbulence interacting with a shock wave are performed for several upstream shock normal Mach numbers (M_1). Turbulence kinetic energy (TKE) is amplified across the shock wave, but this amplification tends to saturate beyond $M_1 = 3.0$. TKE amplification and Reynolds stress anisotropy obtained in DNS are consistent with LIA predictions. Rapid evolution of TKE immediate downstream of the shock wave persists for all shock strengths and is attributed to the transfer between kinetic and potential modes of turbulence energy through acoustic fluctuations. Changes in energy spectra and various length scales across the shock wave are predicted by LIA, which is consistent with DNS results. Most turbulence length scales decrease across the shock. Dissipation length scale ($\bar{\rho}q^3/\epsilon$), however, increases slightly for shock waves with $M_1 < 1.65$. Fluctuations in thermodynamic variables behind the shock wave stay nearly isentropic for $M_1 < 1.2$ and deviate significantly from isentropy for the stronger shock waves due to large entropy fluctuation generated through the interaction.

1. Motivation and objective

The presence of shock waves is an important feature that distinguishes high-speed supersonic flows. Understanding the mechanisms of turbulence interacting with a shock wave is not only of generic interest, but also of fundamental importance in predicting the interactions of turbulent boundary layers with the shock waves which occur in many engineering applications. Since the 1950's, linear analyses (LIA) on the modification of elementary disturbance waves, such as vortical, acoustic, and entropic waves, by the shock wave have been performed with an emphasis on the acoustic wave generation behind the shock wave (Ribner 1953, 1954, 1968, Moore 1953, Kerrebrock 1956, Chang 1957, McKenzie and Westphal 1968). Recently, the applicability of homogeneous Rapid Distortion Theory (RDT) on shock/turbulence interaction was investigated by Jacquin *et al.* (1993).

There has been a significant accumulation of experimental data on the shock turbulence interaction during the last decade. Interaction of turbulent boundary layers with a shock wave over a corner was investigated by many research groups, among them are Dolling and Or (1985), Andreopoulos and Muck (1987), Smits and Muck (1987). A general finding from these experiments is that Reynolds shear stress and turbulence intensities are amplified across the shock wave. The studies of oblique shock wave/turbulent boundary layer interaction included several additional phenomena which complicated the flow behavior (Honkan and Andreopoulos 1992). To isolate the effects of a shock wave on turbulence, several experiments (Debieve and

Lacharme 1986, Keller and Merzkirch 1990, Jacquin *et al.* 1991, Honkan *et al.* 1992) on the interaction between the shock wave and grid-generated turbulence have been performed. They found that turbulence is amplified and turbulence length scales increase across the shock wave. But the length scale increase contradicts the intuitive expectation that mean flow compression should decrease the relevant turbulence length scales. The issue of length scale change will be thoroughly discussed in the present paper (Sec. 2.2).

Numerical simulations of the shock turbulence interaction are just beginning to emerge. Using a shock capturing numerical technique, Rotman (1991) calculated the change in a two dimensional turbulent flow caused by the passage of the traveling shock wave. He found that the shock causes an increase in the turbulent kinetic energy and that the length scale of the turbulent field is reduced upon passage of the shock. Lee *et al.* (1991a, 1992) conducted direct numerical simulations of two and three dimensional turbulence interacting with a shock wave. They found that vorticity amplification compared well with the linear analysis predictions, and turbulent kinetic energy undergoes rapid increase behind the shock wave. The spectrum was found to be enhanced more at large wave numbers, leading to an overall length scale decrease.

In the present report, interaction of isotropic turbulence with a strong shock wave is studied to investigate the effects of shock strength on turbulence modification. A numerical technique to simulate turbulence interacting with a strong shock wave without resolving its structure was developed, and it validated this technique against the shock-resolving simulations (Lee 1993). The simulation results are compared with the results from a linear analysis, and they are contrasted against the results from the weak shock case to show the shock strength effects.

2. Accomplishments

The parameters of the simulation are the mean Mach number (M_1), the fluctuation Mach number (M_t), and the turbulence Reynolds number based on the Taylor microscale (Re_λ) upstream of the shock wave. In the simulation, all of the turbulence scales are fully resolved, while the effect of the shock wave on turbulence is captured (rather than fully resolved). Two new simulations are conducted for the interaction with strong shock waves ($M_1 = 2.0, 3.0$), and the results from shock-resolving simulations (Lee *et al.* 1993) for the interaction with a weak shock wave ($M_1 = 1.05, 1.1, 1.2$) are quoted to investigate the effects of the shock normal Mach number. Table 1 lists the simulation parameters, where the values of M_t and Re_λ are taken at the location immediately upstream of the shock.

Table 1. Parameters for the simulations of shock turbulence interaction

Case	M_1	M_t	Re_λ	k_o
A	2.0	0.108	19.0	4.0
B	3.0	0.110	19.7	4.0

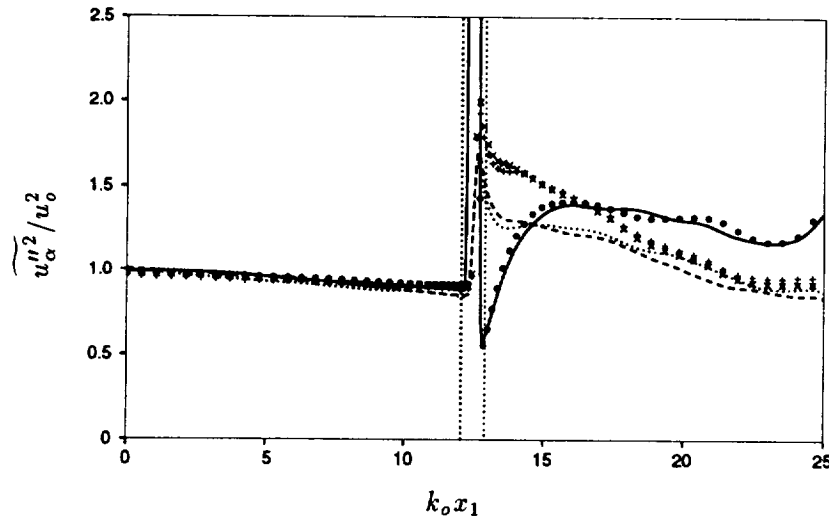


FIGURE 1(A). Evolution of the normal components of the Reynolds stress: lines for $M_1 = 2.0$, and symbols for $M_1 = 3.0$. —, \bullet : R_{11} , ----, \times : R_{22} , , $+$: R_{33} . Vertical lines denote the boundaries of shock intermittency.

2.1 Turbulence velocity fluctuation

Interaction of turbulence with a shock wave generates acoustic waves downstream of the shock, part of which undergo rapid decay (Ribner 1953). LIA predicts that turbulent kinetic energy is amplified across the shock wave and the decaying acoustic waves contribute significantly to the streamwise fluctuations just behind the shock wave.

Figure 1(A) shows the evolution of the diagonal components of the Reynolds stress tensor, $R_{ij} = \overline{u''_i u''_j}$. The off-diagonal components stay close to zero over the entire flow field since turbulence is isotropic upstream and axisymmetric downstream of the shock. The streamwise component in the shock region contains the intermittency effects due to the oscillations of the shock. For more details of the intermittency effects on turbulence statistics, see Lee *et al.* (1992). The boundaries of the shock oscillations are defined as the locations where mean dilatation $d\bar{u}_1/dx_1 = 0$; $d\bar{u}_1/dx_1$ is negative inside the shock wave and slightly positive away from the shock due to viscous heating. All the velocity fluctuations are enhanced during the interaction. The velocity fluctuations are axisymmetric behind the shock, and their return to isotropy is negligible compared to the decay. Away from the shock wave, all the velocity fluctuations decay monotonically due to the viscous dissipation.

Mach number dependence of the far-field velocity fluctuation amplification predicted by LIA is shown in Figure 1(B). All components of the velocity fluctuation are amplified across the shock wave, and the amplification of TKE tends to saturate beyond $M_1 = 3.0$. The shock normal component is amplified more for shock waves with $M_1 < 2.0$ while the opposite is true for $M_1 > 2.0$. In DNS, however, the streamwise velocity fluctuation away from the shock is larger than the transverse velocity fluctuations, which apparently contradicts with the LIA prediction. Viscous

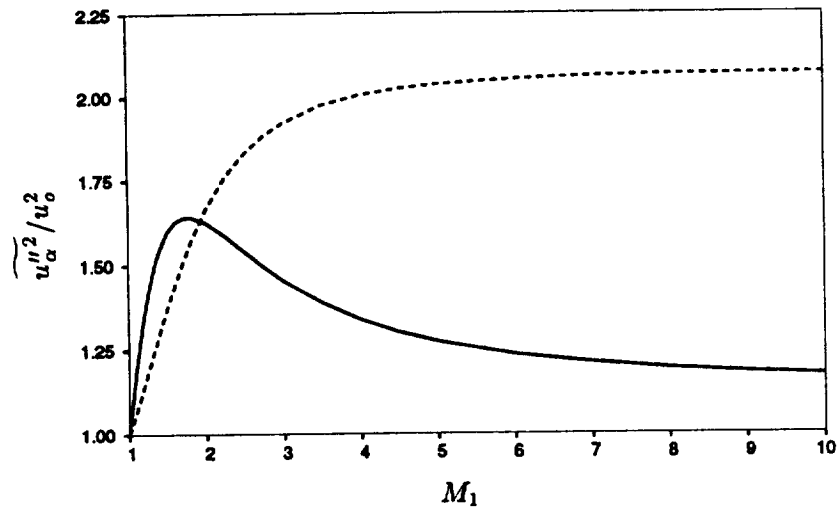


FIGURE 1(B). Amplification of velocity fluctuation variances across the shock wave predicted by LIA at far away from the shock. — $\overline{u_1''^2}$, ---- $\overline{u_2''^2}$ & $\overline{u_3''^2}$.

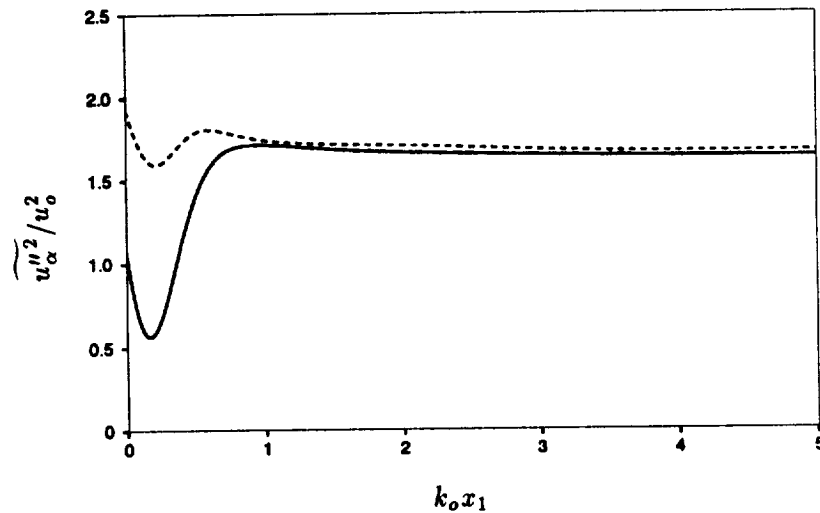


FIGURE 1(C). Evolution of velocity fluctuation variances behind the shock wave predicted by LIA ($M_1 = 2.0$). — $\overline{u_1''^2}$, ---- $\overline{u_2''^2}$ & $\overline{u_3''^2}$.

TKE dissipation rate behind the shock for the transverse components are found to be significantly higher than the streamwise component. Therefore, comparing low Reynolds number DNS results directly with the inviscid linear analysis is not fair. After the viscous decay is compensated for by extrapolating the curves to the shock location, the trend of amplification from the DNS is found to be consistent with the LIA prediction.

The rapid evolution of velocity fluctuations which was observed for weak shock turbulence interaction (Lee *et al.* 1993) persists in the present simulations of strong shock turbulence interaction. In order to understand the downstream evolution of the velocity fluctuations, the budget of the Reynolds stress transport equation downstream of the shock wave is investigated. All terms in the transport equation can be accurately evaluated, since all the flow variables are fully resolved both in time and space outside the shock wave. As for weak shock case, the pressure transport term $(-\overline{p'u''_1})_{,1}$ in the inhomogeneous (or the shock normal) direction is mainly responsible for the rapid evolution of the streamwise velocity fluctuation. The evolution of the velocity fluctuations downstream of the shock wave predicted by LIA is shown in Figure 1(C), which reproduces the main feature of the rapid evolution from the DNS. Hence, the rapid TKE evolution behind the shock wave can be explained mainly as a linear process. This rapid evolution in the streamwise velocity fluctuation is due to a correlation between the vortical and decaying acoustic fluctuations behind the shock wave. The acoustic velocity fluctuations and vortical velocity fluctuations are anti-correlated just behind the shock, and the correlation between the two fluctuations decreases rapidly as the amplitude of the acoustic wave decays exponentially away from the shock wave. In previous studies (Lee *et al.* 1991a, 1992, 1993), the correlations between vortical and acoustic waves were not properly accounted for, and the prediction capability of the linear analysis was not fully appreciated.

Another facet of the rapid evolution of velocity fluctuations is revealed by an equation for linear acoustic energy balance (Thompson 1985). The continuity and momentum equations for the linearized fluctuating components can be written as

$$\begin{aligned}\frac{\partial \rho'}{\partial t} + \tilde{u}_k \frac{\partial \rho'}{\partial x_k} + \bar{\rho} \frac{\partial u''_k}{\partial x_k} &= 0, \\ \frac{\partial u''_i}{\partial t} + \tilde{u}_k \frac{\partial u''_i}{\partial x_k} + \frac{1}{\bar{\rho}} \frac{\partial p'}{\partial x_i} - \frac{\partial \sigma''_{ik}}{\partial x_k} &= 0\end{aligned}$$

by assuming that there exist no mean flow gradients, where $\bar{\rho}\sigma''_{ij}$ ($=\tau''_{ij}$) denotes the viscous stress. For an ideal gas, an infinitesimal density fluctuation can be related to the pressure and entropy (s) fluctuations by

$$\frac{\rho'}{\bar{\rho}} = \frac{1}{\gamma} \frac{p'}{\bar{p}} - \frac{s'}{c_p},$$

where c_p is the specific heat at constant pressure. Multiplying the continuity equation by ρ' , contracting the momentum equations by u''_i , and cancelling density-dilatation correlation by using above thermodynamic relation with neglecting entropy fluctuation effect ($-s'u''_{i,i}/c_p\bar{c}$), the following equation (in the averaged form) follows.

$$\frac{\partial}{\partial x_k} \left[\frac{\tilde{u}_k}{\bar{c}} \left(\frac{\overline{u''_i u''_i}}{2\bar{c}^2} + \frac{\overline{\rho'^2}}{2\bar{\rho}^2} \right) + \frac{1}{\gamma} \frac{\overline{p' u''_k}}{\bar{p} \bar{c}} \right] - \frac{\overline{u''_i \partial \sigma''_{ik}}}{\bar{c}^3 \partial x_k} = 0.$$

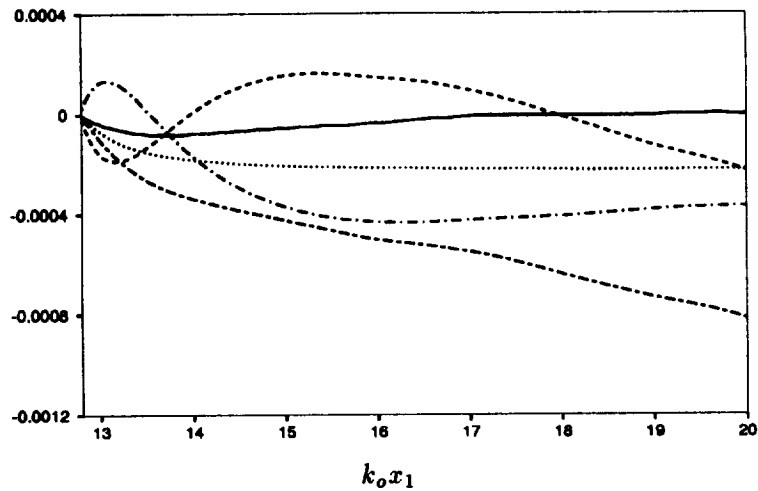


FIGURE 2(A). Evolution of the integrated quantities from the acoustic energy balance for $M_1 = 2.0$: - - - - A , B , - · - · C , - - - - $A + B + C$, ——— $A + B + C + D$.

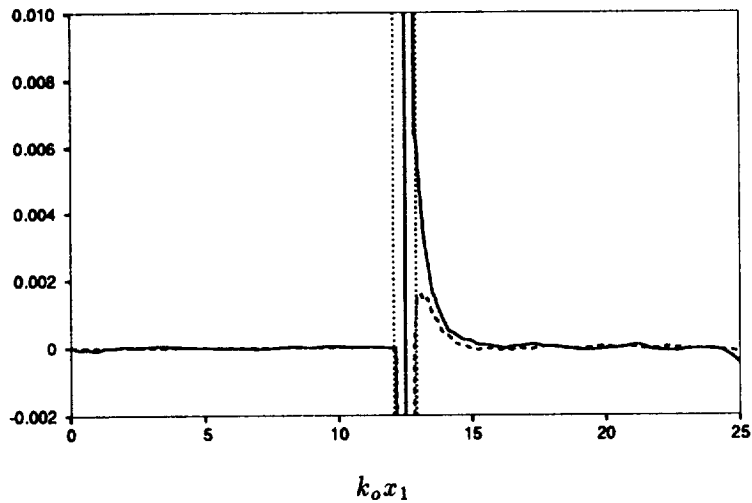


FIGURE 2(B). Evolutions of pressure-dilatation correlation and entropy-dilatation correlation for $M_1 = 2.0$: ——— $\overline{p'u''_{k,k}}/\gamma\bar{p}u_0k_0$, - - - - $-\overline{s'u''_{k,k}}/c_p u_0 k_0$. Vertical lines denote the boundaries of shock intermittency.

If this relation is satisfied the phenomenon can be explained in terms of linear acoustic energy balance.

The acoustic balance equation is integrated in the streamwise direction from the downstream side of the shock (x_s) to give

$$\underbrace{\left\| \frac{\tilde{u}_1}{\bar{c}} \frac{u_i'' u_i''}{2\bar{c}^2} \right\|_{x_s}^{x_1}}_A + \underbrace{\left\| \frac{\tilde{u}_1}{\bar{c}} \frac{\rho'^2}{2\bar{\rho}^2} \right\|_{x_s}^{x_1}}_B + \underbrace{\left\| \frac{1}{\gamma} \frac{p' u_1''}{\bar{p} \bar{c}} \right\|_{x_s}^{x_1}}_C - \underbrace{\int_{x_s}^{x_1} \frac{u_i''}{\bar{c}^3} \frac{\partial \sigma''}{\partial x_k} dx_1}_D = 0,$$

where $\|f\|_a^b = f(b) - f(a)$. The integrated results are shown in Figure 2(A). In all the cases we investigated (with different shock strengths and upstream turbulence intensities) the acoustic energy balance is satisfied with little deviation. The rapidly evolving acoustic energy — sum of scaled density and velocity fluctuations — is found to be mainly balanced by the pressure transport once the decay due to viscous dissipation is compensated. Therefore, the rapid evolution of velocity fluctuations can be attributed to the acoustic energy balance: energy transfer from the acoustic potential energy in the form of density (or pressure) fluctuations to turbulence kinetic energy. This is consistent with the fact that the pressure-transport term is scaled best by flow variables associated with acoustic wave propagation (Lee *et al.* 1993). Note that density fluctuation is replaced by the pressure fluctuation using the isentropic relation in deriving the acoustic energy balance equation, even though entropy fluctuation behind the shock wave contributes significantly to the density fluctuation (as is shown in Sec. 2.3). This is justified because as shown in Figure 2(B) the neglected entropy-dilatation correlation is found to be less than 30% of the pressure-dilatation correlation in the zone of interest, and 5% of the pressure transport term. Even though thermodynamic fluctuations are far from isentropic, the contribution of entropy fluctuations to the acoustic energy balance can be neglected. The entropy-dilatation correlation vanishes in the linear limit and the acoustic energy balance derived above holds exactly in the linear analysis, which ignores viscous dissipation.

Variance of vorticity fluctuation is a main contributor to the TKE dissipation rate. Figure 3(A) shows the evolution of vorticity components. The transverse components are amplified across the shock, while the streamwise component is hardly affected. Mach number dependence of transverse vorticity variance amplification predicted by LIA is shown in Figure 3(B). LIA predicts no amplification of the streamwise component. The amplification trend and its amplification ratio obtained from DNS are found to be consistent with the LIA prediction.

2.2 Turbulence length scales

Experimental studies (Debieve *et al.* 1986, Keller *et al.* 1990, Honkan *et al.* 1992) have reported that large scale turbulent motions are enhanced more than small scale motions as turbulence passes through a shock wave, leading to the overall increase of turbulence length scales, especially of microscales. LIA predicts that Taylor microscales decrease across the shock wave for all shock strengths, which was confirmed by DNS for weak shock waves (Lee *et al.* 1991a, 1993). For weak shock waves, changes in some turbulence length scales were too small to draw definite conclusions on the issue.

To investigate the scale-dependent amplification of turbulence, the modification of power spectra across the shock wave ($M_1 = 2.0$) is computed through LIA for

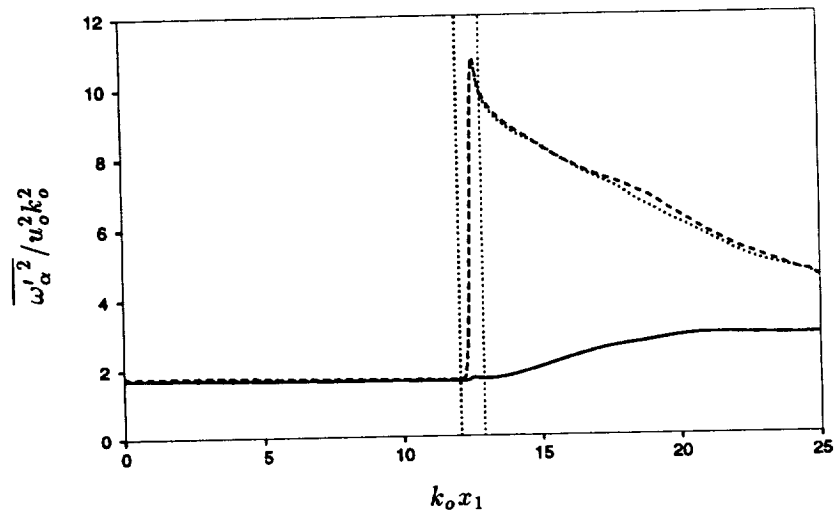


FIGURE 3(A). Evolution of the vorticity fluctuation variances with $M_1 = 2.0$:
 — $\overline{\omega_1'^2}$, - - - $\overline{\omega_2'^2}$, $\overline{\omega_3'^2}$.

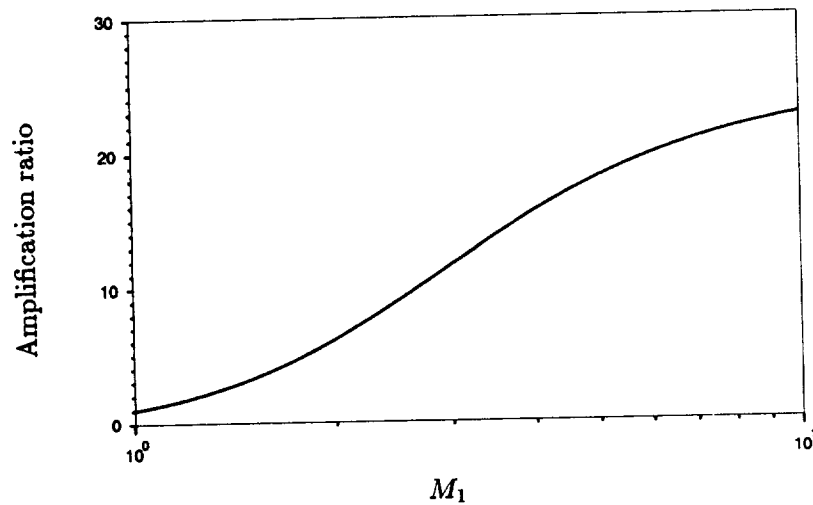


FIGURE 3(B). Amplification of transverse vorticity fluctuation variances predicted by LIA.

the one dimensional spectrum in the shock-normal (longitudinal) and transverse direction which is shown in Figure 4(A) and (B), respectively. In the longitudinal spectrum, significant scale-dependent amplification is observed: more amplification at small scales than at large scales. Large scale part of $E_2(k_1)$ is even suppressed through the interaction. In the transverse spectrum, more amplification at small scales is found for $E_1(k_2)$ and $E_2(k_2)$, while more amplification at large scale is found for $E_3(k_2)$. The energy spectrum used in the analysis is the von Karman

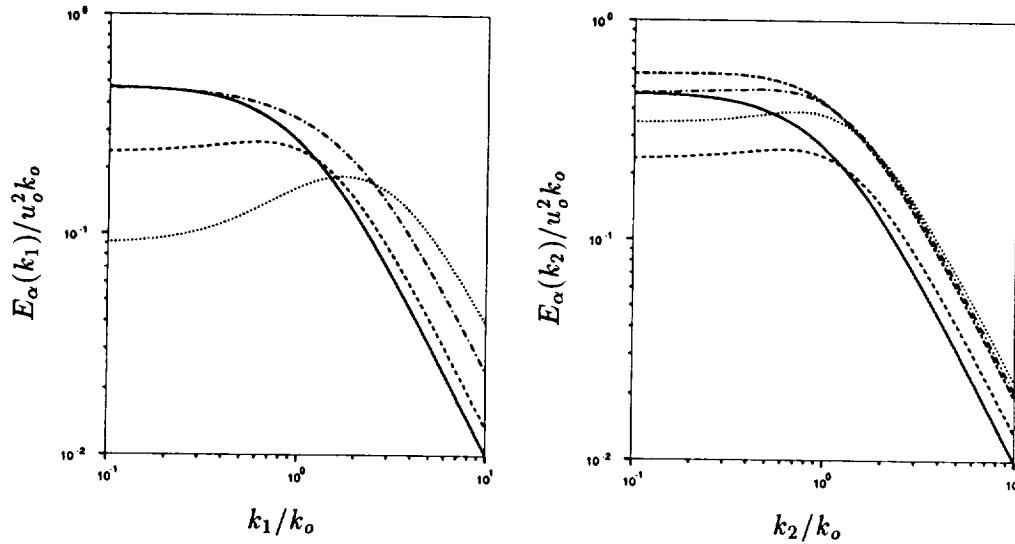


FIGURE 4. (a) LIA prediction of the shock-normal direction (vs. k_1) one dimensional energy spectra change across the shock wave for $M_1 = 2.0$: E_1 : — upstream, — downstream, E_2 & E_3 : ---- upstream, downstream. (b) LIA prediction of the transverse direction (vs. k_2) one dimensional energy spectra change across the shock wave for $M_1 = 2.0$: E_2 : — upstream, — downstream, E_1 : ---- upstream, downstream, E_3 : ---- upstream, ---- downstream.

spectrum (Hinze 1975), but the results obtained in the analysis are insensitive to choice of the spectrum. Since the spectrum amplification pattern is different for different spectrum (e.g. $E_1(k_2)$ or $E_3(k_2)$), the issue of the length scale change should be addressed for the specific length scale only. In the following, changes in various turbulence length scales are discussed.

To directly check the scale-dependent turbulence amplification, transverse power spectra of velocity fluctuations in a numerically simulated field from case A are shown for upstream and downstream of the shock wave in Figure 5. Amplification is more pronounced at the large wave numbers, which is consistent with the prediction by the linear analysis in Figure 4(B).

Keller *et al.* (1990) reported that both the density microscale and the integral length scale in the shock normal direction increase for shock waves with $M_1 < 1.24$. In the present simulation, the spectrum changes of density and temperature fluctuations across the shock are found to be similar to those of velocity fluctuations: Spectrum is amplified more at small scales than at large scales. The difference between the present study and the experiment may be due to the assumptions made in the experimental data analysis, such as turbulence isotropy/homogeneity, and negligible pressure fluctuations, which may be too crude in light of the simulation. Velocity fluctuation variances are axisymmetric as shown in Sec. 2.1, and thermodynamic property fluctuations are not isobaric and decay rapidly behind the shock wave as shown in Sec. 3.3. The effects of these imperfect assumptions on the data

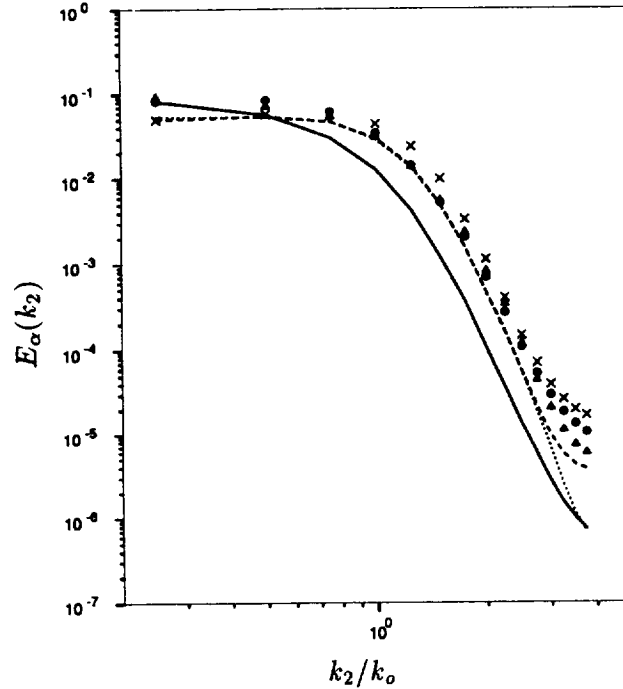


FIGURE 5. Changes in one dimensional spectra across the shock wave which is at $k_0 x_s = 12.29$: lines for upstream spectra at $k_0 x_1 = 10.59$, and symbols for downstream spectra at $k_0 x_1 = 13.68$. —, \bullet : $E_2(k_2)$, ----, \times : $E_1(k_2)$, , \triangle : $E_3(k_2)$.

analysis are not clearly documented in Keller *et al.* (1990).

Figure 6(A) shows the evolutions of Taylor microscales (λ_α) and the transverse density microscale (λ_ρ), which are defined as

$$\lambda_\alpha = \frac{\sqrt{u_\alpha'^2}}{\sqrt{u_{\alpha,\alpha}'^2}} \quad \text{and} \quad \lambda_\rho = \frac{\sqrt{\rho'^2}}{\sqrt{\rho'_{,2}{}^2}},$$

respectively. All the microscales decrease significantly across the shock wave: the streamwise Taylor microscale by about 50%, the transverse Taylor microscales by about 20%, and the density microscale by about 30%. Mach number dependence of Taylor microscale change predicted by LIA is shown in Figure 6(B). The higher the Mach number, the Taylor microscales are reduced further through the shock wave. The reduction is more pronounced in the shock-normal direction. The reduction observed in the simulation agrees well with the LIA prediction. The Taylor microscale which was reported to increase (Debieve *et al.* 1986) was the time scale, not the length scale (Debieve 1992, private communication). If the mean velocity decrease across the shock is properly accounted for, their experimental result is consistent with the present simulation and analysis.

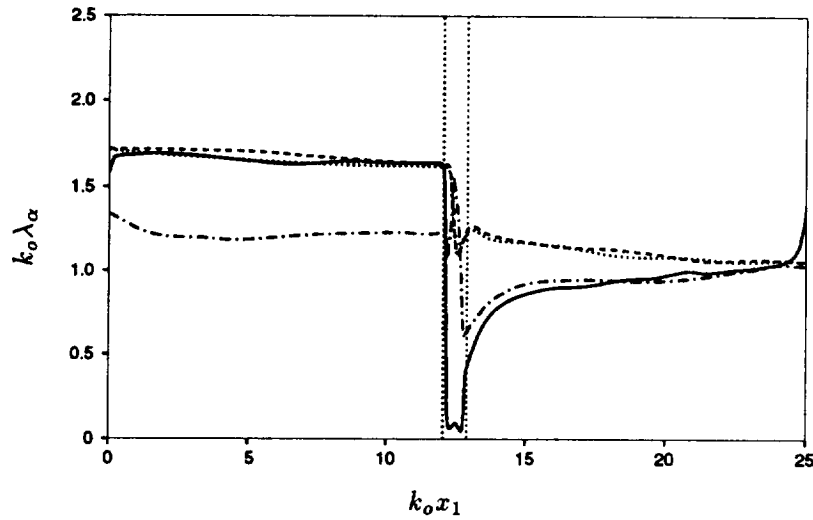


FIGURE 6(A). Evolution of microscales throughout the computational domain for $M_1 = 2.0$: — λ_1 , ---- λ_2 , λ_3 , —·— λ_ρ . Vertical lines denote the boundaries of shock intermittency.

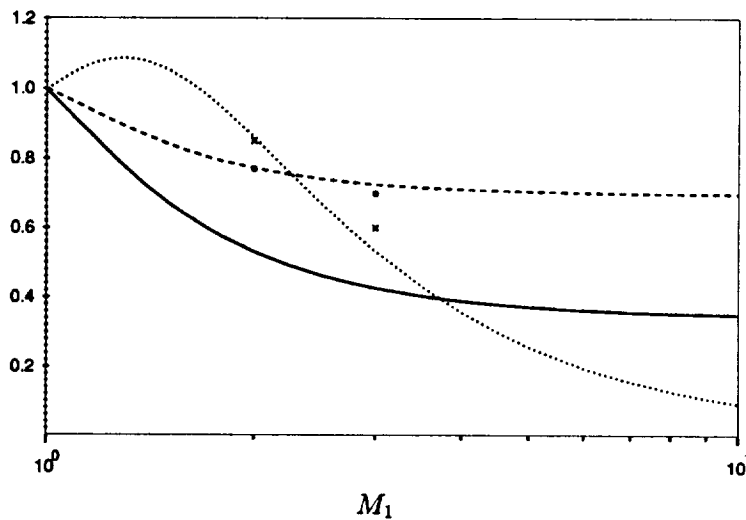


FIGURE 6(B). Change of Taylor microscales and dissipation length scale across the shock wave predicted by LIA. — λ_1 , ---- λ_2 & λ_3 , l_ϵ . Symbols for DNS: ● λ_2 , × l_ϵ .

Integral scale (Λ_f) of turbulent fluctuation f' in the x_2 -direction is defined from its two-point correlation, $C_f(r; x_1)$, defined as

$$C_f(r; x_1) = \frac{\overline{f'(x_1, x_2, x_3, t)f'(x_1, x_2 + r, x_3, t)}}{\overline{f'(x_1, x_2, x_3, t)f'(x_1, x_2, x_3, t)}}$$

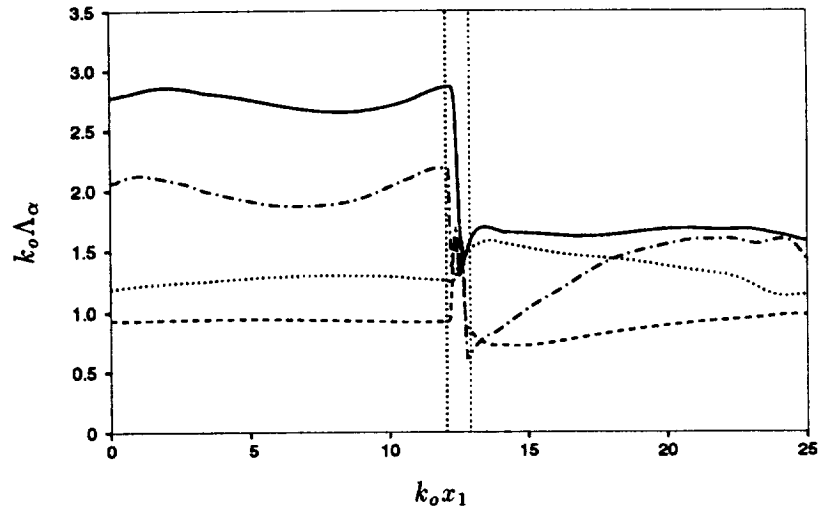


FIGURE 7. Evolution of integral scales throughout the computational domain for $M_1 = 2.0$: — Λ_{u_2} , --- Λ_{u_1} , Λ_{u_3} , —·— Λ_ρ . Vertical lines denote the boundaries of shock intermittency.

where the average is taken over time and homogeneous directions (x_2 - and x_3 -directions). The integral scale (Λ_f) is, then, defined as

$$\Lambda_f(x_1) = \int_0^\infty C_f(r; x_1) dr,$$

where the upper limit of the integration is replaced by $L/2$ when dealing with numerically simulated field with L being the computational box size in the x_2 -direction, where the periodic boundary condition is enforced. Figure 7 shows the evolutions of four integral scales throughout the flow field. Three integral scales (Λ_{u_1} , Λ_{u_2} , and Λ_ρ) undergo reductions across the shock wave, most significantly in Λ_{u_2} by about 45%, while Λ_{u_3} increases by about 30%. Mach number dependence of the integral length scale change can be predicted by LIA. For the shock wave with $M_1 = 2.0$, the ratio of the downstream to the upstream integral length scale (with the von Karman upstream spectrum) is 0.91, 0.60, 1.46 for Λ_{u_1} , Λ_{u_2} , and Λ_{u_3} , respectively. The simulation results agree well with the LIA predictions considering the difference in the upstream energy spectrum shape (see Fig. 4).

Most widely used length scale in turbulence modelling is the dissipation length scale (l_ϵ), defined as

$$l_\epsilon = \bar{\rho} q^3 / \epsilon,$$

where ϵ is the dissipation rate of turbulence kinetic energy, which includes contributions from both solenoidal and dilatational motions. Figure 8 shows the evolution of the length scale l_ϵ . The dissipation length scale also decreases across the shock wave. Just behind the shock wave, the length scale undergoes rapid increase as was the case with the streamwise Taylor microscale (Figure 6(A)), due to the rapid

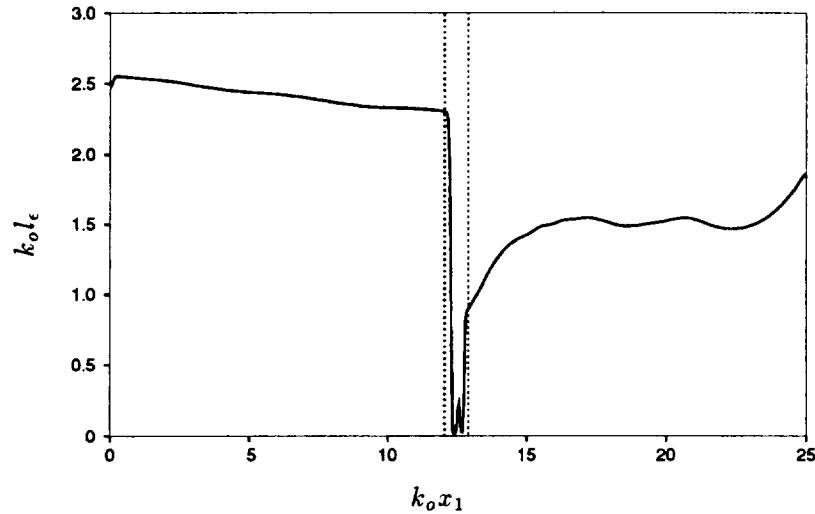


FIGURE 8. Evolution of the dissipation length scale throughout the computational domain for $M_1 = 3.0$. Vertical lines denote the boundaries of shock intermittency.

decay of the acoustic waves (or, the dilatational motions). The Mach number dependence of the dissipation length scale change predicted by LIA is presented in Figure 6(B). The length scale is reduced for strong shock waves, while it shows a mild increase for shock waves with $M_1 < 1.65$. For weak shock waves, TKE and its dissipation rate is comparably amplified to give slight increase in l_e across the shock wave, while TKE amplification saturate much faster than vorticity variance amplification to give the reduction in the length scale (Lee *et al.* 1993). The length scale increase observed by Honkan *et al.* (1992) at $M_1 = 1.24$ (the equivalent shock normal Mach number in their experiment is 1.24 not 1.62) might be explained as the phenomenon occurring for weak shock waves, but the analyzed experimental results are not in quantitative agreement with the simulation and the analysis: LIA predicts less than 10% increase, while the analyzed experimental data shows more than 600% increase. This difference seems to suggest that the assumptions used in the experimental data analysis may be too crude, such as negligence of pressure fluctuations and applicability of Taylor's hypothesis in high intensity turbulence, and should be examined carefully.

2.3 Thermodynamic quantities

Thermodynamic fields which are obtained from the freely decaying turbulence (Lee *et al.* 1991b) and prescribed at the inflow are nearly isentropic. As the flow passes through the shock wave, all the fluctuations are amplified, followed by a decay. A general assumption on the relation between thermodynamic fluctuations is polytropic (with a polytropic exponent n), where

$$\frac{p'}{\bar{p}} = n \frac{\rho'}{\bar{\rho}} = \frac{n}{n-1} \frac{T''}{\bar{T}}.$$

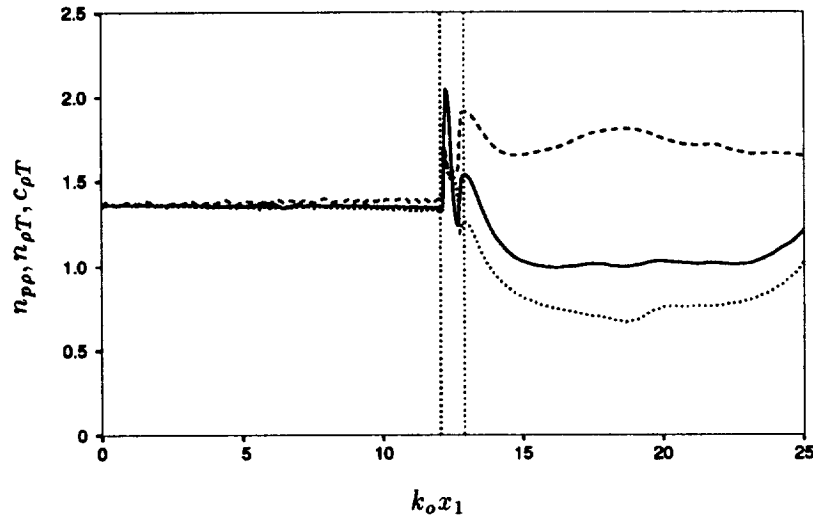


FIGURE 9. Evolution of exponents for the fluctuations in thermodynamic variables for $M_1 = 2.0$: — $n_{p\rho}$, ---- $n_{\rho T}$, $c_{\rho T}$. Vertical lines denote the boundaries of shock intermittency.

For polytropic fluctuations, specification of one property fluctuation and the polytropic exponent is enough to describe the thermodynamic fluctuations. Based on the above relations, different polytropic exponents can be defined using normalized rms fluctuations ($n_{p\rho}, n_{\rho T}$) and the correlations between instantaneous fluctuations ($c_{\rho T}$) as

$$n_{p\rho} = \frac{\sqrt{\overline{p'^2}/\bar{p}}}{\sqrt{\overline{\rho'^2}/\bar{\rho}}}, \quad n_{\rho T} = 1 + \frac{\sqrt{\overline{T'^2}/\bar{T}}}{\sqrt{\overline{\rho'^2}/\bar{\rho}}},$$

and

$$c_{\rho T} = 1 + \frac{\bar{\rho}}{\bar{T}} \frac{\overline{\rho' T''}}{\bar{\rho}^2}.$$

For weak shock waves with $M_1 \leq 1.20$, relations between thermodynamic property fluctuations are close to isentropic ($n = \gamma$) throughout the flow field (Lee *et al.* 1993).

In order to check the polytropy for the strong shock case, the polytropic exponents, $n_{p\rho}, n_{\rho T}$, defined above are investigated. If the fluctuations are indeed polytropic, the two exponents should be the same, which is defined as the polytropic exponent. The evolutions of the two exponents are shown in Figure 10. The exponents are the same upstream of the shock wave with $n_{p\rho} = n_{\rho T} \simeq \gamma$. Downstream of the shock wave, however, they differ significantly with $n_{p\rho}$ decreasing and $n_{\rho T}$ increasing. Their return to polytropy is very slow. To further investigate the relation between instantaneous fluctuations, the correlation between the fluctuations of density and temperature ($\overline{\rho' T''}$) is studied.

The evolution of the exponent is also shown in Figure 9. Upstream of the shock wave, the exponent is quite close to the $\gamma (= 1.40)$. It drops significantly across the shock wave, and its further evolution is rather slow. The change in the exponents across the shock wave is found to be consistent with the LIA prediction (shown in Figure 10). Upstream thermodynamic fluctuations are polytropic (close to isentropic), and downstream fluctuations are not isentropic due to significant entropy fluctuations produced by the shock turbulence interaction. To properly describe the thermodynamic fluctuations in strong shock turbulence interaction, specification of at least one thermodynamic fluctuation along with two exponents (*i. e.*, $n_{p\rho}$ and $n_{\rho T}$) are required.

The shock strength effects on thermodynamic fluctuations for wider range of shock normal Mach numbers can easily be investigated through the linear analysis. In the following, polytropic exponents downstream of the shock in the interaction of solenoidal velocity fluctuations with a shock wave is studied. The effects of the shock strength on downstream polytropic exponents are shown in Figure 10. For isentropic or acoustic fluctuations, all the exponents are same and equal to the specific heat ratio. For entropic or isobaric fluctuations, $n_{p\rho}$ and $c_{\rho T}$ become 0 and $n_{\rho T}$ becomes 2. For weak shock waves with $M_1 < 1.2$, thermodynamic fluctuations behind the shock can be regarded as isentropic. As the shock becomes stronger beyond this limit, the entropy fluctuation behind the shock cannot be neglected, and its importance becomes more dominant for the stronger shock waves. The results of the polytropic exponents from DNS are consistent with LIA predictions with the values from DNS systematically deviating from the LIA predictions toward the isentropic value of 1.4. This may be due to (incompressible) pressure fluctuations associated with dilatation-free velocity fluctuations (Sarkar *et al.* 1991), which accompany mainly isentropic thermodynamic fluctuations.

In order to quantify the importance of entropy fluctuations behind the shock wave, the contributions of acoustic and entropic fluctuations to the density fluctuation are quantified by the linear analysis and also shown in Figure 10. Since the acoustic fluctuations and entropic fluctuations are completely decorrelated in the linear limit, the relative importance of entropy fluctuations can be expressed as $\frac{\overline{s'^2}/c_p^2}{\overline{\rho'^2}/\bar{\rho}^2}$. For weak shock waves with $M_1 < 1.2$, entropy fluctuations contribute less than 2% to the density fluctuations. However, entropy fluctuations become more important than acoustic fluctuations beyond $M_1 = 1.65$.

In summary, thermodynamic fluctuations downstream of the shock wave are found to be isentropic for weak shock waves ($M_1 < 1.2$) and become non-polytropic for strong shock waves, where the importance of entropy fluctuations are comparable to the acoustic fluctuations. The thermodynamic fluctuations cannot be modelled using polytropic exponents in this regime. Therefore, modelling effort should be made separately for the acoustic fluctuations and entropic fluctuations. Zeman (1993) stressed the need for such a separation for the mean thermodynamic quantities.

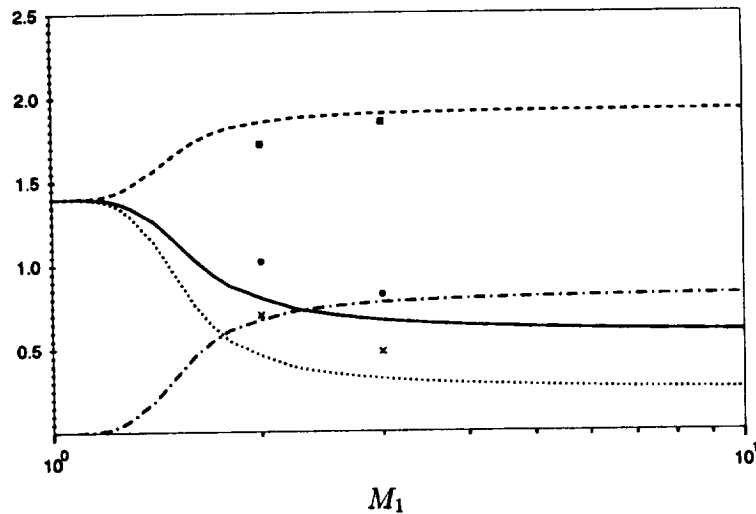


FIGURE 10. Downstream polytropic exponents and entropy fluctuation contribution predicted by LIA. — $n_{p\rho}$, - - - $n_{\rho T}$, $c_{\rho T}$, - · - Entropy fluctuation contribution. Symbols for DNS: ● $n_{p\rho}$, □ $n_{\rho T}$, × $c_{\rho T}$.

3. Future plans

The varied evolution of thermodynamic variables in Large-eddy Simulation (LES) using different formulations (where no explicit removal of aliasing errors is performed) has not yet been understood. In order to have a reference case where aliasing errors are removed exactly, a specific volume formulation in solving compressible Navier-Stokes equations is being pursued. Large eddy simulation of isotropic turbulence with a shock wave will be performed once the cause for the difference in the evolution of thermodynamic quantities is better understood.

Numerical simulation will be extended for a more practical situation where the turbulent boundary layer is subjected to externally imposed strains: a boundary layer under rapid expansion and over a compression ramp.

This work was produced in collaboration with Prof. S. Lele and Prof. P. Moin.

REFERENCES

- ANDREOPOULOS, J. & MUCK, K.-C. 1987 Some New Aspects of the Shock-Wave Boundary Layer Interaction in Compression Ramp Corner. *J. Fluid Mech.* **180**, 405-428.
- CHANG, C.-T. 1957 Interaction of a Plane Shock Wave and Oblique Plane Disturbances with Special Reference to Entropy Waves. *J. Aero. Sci.* **24**, 675-682.
- DOLLING, D. S. & OR, C. T. 1985 Unsteadiness of the Shock Wave Structure in Attached and Separated Compression Ramp Flows. *Exp. Fluids.* **3**, 24-32.
- DEBIEVE, J. F. & LACHARME, J. P. 1986 A Shock-Wave/ Free Turbulence Interaction. *Turbulent Shear Layer/ Shock Wave Interactions*, J. Délerly (ed.), Springer, Berlin.

- FAVRE, A. 1965 Équations des gaz turbulents compressibles I. *Journal Mécanique*. **4**, 361-390.
- GILES, M. B. 1990 Nonreflecting Boundary Conditions for Euler Equation Calculations. *AIAA Journal*. **28**, 2050-2058.
- HINZE, J. O. 1975 *Turbulence*, McGraw-Hill, p. 247.
- HONKAN, A. & ANDREOPOULOS, J. 1992 Rapid Compression of Grid-Generated Turbulence by a Moving Shock Wave. *Phys. Fluids A*. **4**, 2562-2572.
- JACQUIN, L., BLIN, E., & GEFFROY, P. 1991 Experiments on Free Turbulence/ Shock Wave Interaction. *Eighth Symposium on Turbulent Shear Flows, Munich*.
- JACQUIN, L., CAMBON, C., & BLIN, E. 1993 Turbulence Amplification by a Shock Wave and Rapid Distortion Theory. *Phys. Fluids A*. **5**, 2539-2550.
- KELLER, J. & MERZKIRCH, W. 1990 Interaction of a Normal Shock Wave with a Compressible Turbulent Flow. *Exp. Fluids*. **8**, 241-248.
- KERREBROCK, J. L. 1956 The Interaction of Flow Discontinuities with Small Disturbances in a Compressible Fluid. *Ph.D. Thesis*. California Institute of Technology.
- LEE, S. 1993 Large Eddy Simulation of Shock Turbulence Interaction. *Annual Research Briefs-1992*, Center for Turbulence Research, Stanford Univ./NASA Ames.
- LEE, S., LELE, S. K., & MOIN, P. 1991a Direct Numerical Simulation and Analysis of Shock Turbulence Interaction. *AIAA Paper No. 91-0523*, Reno, Nevada.
- LEE, S., LELE, S. K., & MOIN, P. 1991b Eddy Shocklets in Decaying Compressible Turbulence. *Phys. Fluids A*. **3**, 657-664.
- LEE, S., MOIN, P., & LELE, S. K. 1992 Interaction of Isotropic Turbulence with a Shock Wave. *Report TF-52*, Department of Mechanical Engineering, Stanford University.
- LEE, S., LELE, S. K., & MOIN, P. 1993 Direct Numerical Simulation of Isotropic Turbulence Interacting with a Weak Shock Wave. *J. Fluid Mech.* **251**, 533-562.
- LELE, S. K. 1992 Compact Finite Difference Schemes with Spectral-Like Resolution. *J. Comp. Phys.* **103**, 16-42.
- MCKENZIE, J. F. & WESTPHAL, K. O. 1968 Interaction of Linear Waves with Oblique Shock Waves. *Phys. Fluids*. **11**, 2350-2362.
- MEADOWS, K. R., CAUGHEY, D. A., & CASPER, J. 1993 Computing Unsteady Shock Waves for Aeroacoustic Applications. *AIAA Paper No. 93-4329*, Long Beach, CA.
- MOORE, F. K. 1953 Unsteady Oblique Interaction of a Shock Wave with a Plane Disturbances. *NACA TN-2879*.
- RIBNER, H. S. 1953 Convection of a Pattern of Vorticity through a Shock Wave. *NACA TN-2864*.

